Chapter 1

Introduction

1.1 The Lunar Topography

The surface of the Moon has been the subject of telescopic investigations for hundreds of years, ever since the earliest instruments were first turned to the night sky (*Whitaker*, 2003), and long before the word "science" came into popular use (*Lindberg*, 1992). Our natural satellite is also the most visited planetary body by spacecraft, aside from the Earth itself, and the only destination (so far) to have been reached by human explorers. The Moon thus occupies a special place in the public imagination, and the shape and properties of its surface in particular have played a significant role in several major scientific debates of the last few decades, including the origin of the Earth-Moon system, the history of life and mass extinctions on our own planet, and the evolution of planetary surfaces throughout the solar system. In 1610, when Galileo first described the pattern of light and shadow he saw through his telescope as the interaction of sunlight with a rugged, three-dimensional terrain (*Galilei*, 1989), he began what has become a long tradition of seeking to decipher the "cuneiform writings" (*Fauth*, 1909) encoded in the lunar surface—that is, to interpret its physical features.

The topography of a planetary body contains the remnants of the geologic, geomorphologic, and cosmic processes that have contributed to its formation and subsequent modification. On the Moon, impact cratering is the dominant agent of surface modification (*Melosh*, 1989), although evidence of other processes, including vast volcanic plains and tectonic features like extensional graben and wrinkle ridges, is also abundant (*Wilhelms et al.*, 1987). Compared to the Earth, with its plate tectonics, atmosphere, and hydrologic cycle, the Moon thus presents a somewhat simplified setting in which to study the most ubiquitous process in the solar system, the collision of bolides with planetary surfaces and the formation of impact craters. Moreover, the lunar surface contains a record of times long past, the corresponding terrestrial record of which has been almost completely erased. The second quote in the dedication of this thesis was written by Ernst J. Öpik in his 1916 paper exploring the possibility that the lunar craters were formed by impact, rather than volcanic, processes. While he concludes that an impact origin is unlikely given the absence of similar features on Earth, he makes an eloquent observation that, to a great extent, describes our current approach toward lunar impact crater studies: the lunar surface is telling of conditions in the past, and that information can be used to interpret cratered terrains throughout the solar system.

This thesis focuses on two parallel approaches to understanding the lunar topography: on the one hand, we employ high-resolution elevation data from recent spacecraft missions to analyze the statistical properties of surface roughness, while on the other, we develop a cratered-terrain model to investigate the expected statistical signatures produced by the process of impact cratering. In developing and comparing these two approaches, our goal is to determine the extent to which the topographical markers of competing geomorphological processes can be disentangled for the Moon, with the hope that improving our understanding of the cratering record on our own satellite will provide a useful resource for other planetary surfaces.

1.1.1 Interpreting Cratered Terrains

Craters were among the first lunar features to be described by early observers, although the word "crater" was only applied to them in the late-18th century, first by Johann Schröter, who borrowed the term from volcanology. This conflation of terms was not accidental, as Schröter, along with most of his contemporaries, believed the lunar craters to be of volcanic origin, based on analogy with terrestrial features. Various versions of the impact theory for the origin of lunar craters were also proposed, but they found little support until the early 20th century, when, fueled by new wartime experiences with aerial reconnaissance and bomb craters, the explosive nature of the impact process began to be explored (*Ives*, 1919; *Gifford*, 1924; *Wegener and Şengör*, 1975). In the decades leading up to the First World War, the debate over lunar craters was fought on two fronts, as both the reliability of terrestrial analogy as a means of interpreting extraterrestrial features and the utility of laboratory-scale impact experiments were contested. The explosion hypothesis provided an explanation for the near-perfect circularity of lunar craters, a common stumbling block for the impact hypothesis because oblique impact angles were known to be more likely than vertical ones (*Gilbert*, 1893) and small-scale experiments commonly resulted in elliptical craters. At the same time, the identification of terrestrial impact craters, especially Meteor Crater in Arizona, led to a broader understanding of the Earth's own impact history (*Hoyt*, 1987). Further developments in the 1940s by *Dietz* (1946), who studied changes in physiographic form with increasing crater diameter, and by *Baldwin* (1949), who connected the depth-diameter scaling for impact craters and chemical explosion craters, established a quantitative relationship between impact energy and crater morphometry (*Doel*, 1996). Detailed studies of nuclear test craters and Meteor Crater led Eugene M. Shoemaker to spearhead the founding of the Astrogeology branch of the United States Geological Survey (USGS) and to initiate the first geologic maps of the Moon (*Shoemaker*, 1963, 1977; *Shoemaker and Hackman*, 1962; *Wilhelms*, 1993).

The recognition that stratigraphic relationships between geologic units of different ages can be determined by close examination of the lunar surface forms the basis of our present understanding of the Moon's surface history. Five major periods, primarily defined by the formation of major basins and the emplacement of mare basalts, are distinguished, the boundaries of which are calibrated by absolute ages from lunar samples: Copernican (~ 1.1 Gya-present), Eratosthenian ($\sim 3.2-1.1$ Gya), Imbrian ($\sim 3.85 - 3.2$ Gya), Nectarian ($\sim 3.9 - 3.85$ Gya), and Pre-Nectarian ($\sim 4.5 - 3.9$ Gya) (*Wilhelms et al.*, 1987; *Stöffler and Ryder*, 2001).

The comparison of crater densities on different surfaces provides a system of relative ages that can be referenced to the absolute ages from radiometric dating of returned samples and lunar meteorites (*Hartmann*, 1970; *Neukum et al.*, 1975; *Strom*, 1977). Statistical treatments of the size-frequency distribution of lunar craters were first derived from telescopic observations of the near side of the

Moon (*MacDonald*, 1931; *Young*, 1940; *Öpik*, 1960; *Baldwin*, 1964), and more detailed studies became feasible in the mid-1960s with the return of photographs from successful lunar probes in the Ranger and Surveyor programs (*Brinkmann*, 1966; *Jaffe*, 1967). Since that time, the interpretation of cratered terrains from a statistical standpoint has developed into a fruitful subfield with its own terminology, conventions, and literature (*Melosh*, 1989), and it now encompasses the study of planetary surfaces across the solar system (*Passey and Shoemaker*, 1982; *Zahnle et al.*, 2003; *Pike*, 1988; *Neukum and Ivanov*, 1994). Detailed examinations of cratered surfaces establish a geologic timescale correlated across planetary bodies (*Shoemaker et al.*, 1961), to determine the populations of impactors responsible for forming them (*Ivanov et al.*, 2002), and to thus provide constraints on dynamical models of solar system formation (*Bottke Jr et al.*, 2005).

1.1.2 Surface Roughness

The term "surface roughness" has generally been used since the 19th century to convey the degree to which an interface—whether it be the outer surface of a rock outcrop (*Shaler and Davis*, 1881), a metal tool (*Nasmyth and Carpenter*, 1874), or bone (*Adams*, 1874)—departs from a perfectly smooth surface. The development of aerial photography and radar in the early 20th century marked the origins of remote sensing as it is practiced today (*Campbell*, 2002), and led to new ways of quantifying the surface roughness of natural terrains and relating these measures to surface processes. In the 1970s, range-Doppler and radar techniques for quantifying surface roughness on planetary bodies came into their own, and techniques were developed to integrate ground-based and spacecraft observations (*Butrica*, 1996; *Ostro*, 1993). By the time laser altimetry was developed for Apollo 15 to measure topographic profiles from orbit (*Kaula et al.*, 1974), multiple kinds of elevation data were available for the Moon.

Today, surface roughness is still defined in a variety of ways, depending on the dataset used, the surface being investigated, and the purpose of the study (*Shepard et al.*, 2001; *Kreslavsky et al.*, 2013). Nevertheless, the quantification of roughness properties has proven highly useful in discriminating among geologic units and understanding the complex interaction between surface processes acting at different scales. On Mars, for example, *Kreslavsky and Head* (2000) found a systematic variation in the Hurst exponent (a unit of measure that captures the scale dependence of slopes, described in Chapter 2) with latitude that has been associated with the presence of subsurface ice. *Aharonson et al.* (1998) and *Aharonson et al.* (2001) found the extreme smoothness of sedimented basins on Mars, especially Amazonis Planitia, to be most analogous to heavily sedimented fluvial basins on Earth, such as the ocean floor. Power spectra of topography were used by *Nimmo et al.* (2011) to study the lithospheres of icy satellites, and *Zuber et al.* (2000) considered surface slopes on asteroid 433 Eros to classify it as a rubble pile. On the Moon, *Rosenburg et al.* (2011) and *Kreslavsky et al.* (2013) found significantly different behavior in roughness properties above and below approximately kilometer scales, with important implications for competing surface processes such as the the emplacement of craters, the generation of lunar regolith through impact gardening, and seismic shaking in the vicinity of large impacts.

1.1.3 Planetary Surface Topography from Laser Altimetry

For planetary applications, laser altimetry relies on the accurate detection and timing of laser pulses reflected from a planetary surface, as well as accurate tracking of spacecraft position from Earth. Thus, orbit determination is the main source of error in the resulting measurements, which are based on the travel time of the emitted and reflected pulses (*Neumann*, 2001). The vertical precision with which each measurement within an orbit track can be made provides a separate, generally smaller, source of error, and the frequency of laser pulses determines the along-track spacing of the elevation measurements (*Smith et al.*, 2010a).

Table 1.1 contains a summary of performance parameters for selected laser altimeters carried on planetary missions. The first instruments were designed for Apollo 15, 16, and 17, and they measured the height of the command and service module at intervals of 30 to 43 km (*Kaula et al.*, 1974). From February through May of 1994, the Clementine orbiter mapped the topography of the Moon (*Smith et al.*, 1997; *Zuber et al.*, 1994), while the Shuttle Laser Altimeter 1 and 2 (SLA-01 and SLA-02) measured the Earth's topography on STS-72 and STS-85, respectively (*Garvin et al.*, 1998). The

Mission Name	Launch Date	Firing Rate (Hz)	Horizontal Accuracy	Vertical Precision	Vertical Accuracy
Apollo 15, 16, 17[a]	1971-1972	0.06	30 km	4 m	400 m
Clementine[a]	1994	0.6	3 km	40 m	90 m
SLA-01[a]	01/1996	10	40 m	0.75 m	2.78 m
SLA-02[a]	08/1997	10	40 m	0.75 m	6.74 m
NLR[a]	02/1996	1-2	20 m	0.31 m	10 m
MOLA[a]	11/1996	10	100 m	0.38 m	1 m
MLA[b]	08/2004	8	15-100 m	1 m	20 m
Kaguya[c]	09/2007	1	50 m	5 m	1 m
Chang'e 1[d]	10/2007	1	30 m	50-100 m	1 m
LOLA[e]	06/2009	28	50 m	10 cm	1 m

Table 1.1: Comparison of laser altimeters flown on planetary missions, from [a]*Neumann* (2001), [b]*Zuber et al.* (2012b); *Smith et al.* (2012), [c]*Araki et al.* (2009), [d]*Li et al.* (2010); *Ping et al.* (2009), and [e]*Smith et al.* (2010a); *Barker et al.* (2014).

NEAR Laser Rangefinder (NLA) was carried on NEAR Shoemaker, a spacecraft that orbited asteroid 433 Eros several times before touching down on the surface (*Zuber et al.*, 2000). The Mars Orbiter Laser Altimeter (MOLA), launched in November of 1996, provided the first global topographic dataset from laser altimetry for Mars (*Smith et al.*, 2001). The Mercury Laser Altimeter (MLA) was launched in 2004 on the MESSENGER (MErcury Surface, Space ENvironment, GEochemistry, and Ranging) spacecraft and, following two flybys in 2008, entered orbit around Mercury in March of 2011. Both the Japan Aerospace Exploration Agency (JAXA) and the Chinese Lunar Exploration Program launched lunar missions in 2007, Kaguya and Chang'e 1, respectively, and each mission carried a laser altimeter (*Araki et al.*, 2009; *Li et al.*, 2010; *Ping et al.*, 2009).

The Lunar Reconnaissance Orbiter (LRO) was launched in June of 2009, carrying the Lunar Orbiter Laser Altimeter (LOLA), the first multibeam laser altimeter designed to measure planetary surface topography (*Smith et al.*, 2010a). A diffractive optical element splits a single laser beam into five output beams, each of which illuminates a 5-m-diameter spot on the surface, and the backscattered pulses are detected and stored independently by the receiver (*Smith et al.*, 2010b). The 28-Hz pulse repetition rate results in a total sampling rate of 140 measurements per second, and, to date, more than 6.3 billion elevation measurements have been recorded (*Barker et al.*, 2014). Successive laser shots are separated by approximately 57 m, and the smallest distance between spots is 25 m (see Figure 2.1). The 5-spot pattern allows for calculation of surface slopes both between laser shots (along-track) and within individual spots in two orthogonal directions, for the first time providing an estimate of the true gradient at one particular scale (*Rosenburg et al.*, 2011). LOLA's high firing rate, multispot pattern, and high precision and accuracy have provided an unprecedented topographic dataset for the Moon that is well suited for investigations of surface roughness and the statistics of cratered terrains like those presented in the following chapters.

1.2 Chapter Overview

This thesis focuses on two interrelated aspects of the lunar topography: impact cratering and surface roughness. The former is the dominant agent of lunar surface modification, both today and throughout most of the Moon's history (*Wilhelms et al.*, 1987). The process of impact cratering and the landscapes it creates have been extensively studied in terms of size-frequency distributions of craters and their implications for relative surface ages (*Shoemaker and Hackman*, 1962; *Neukum et al.*, 1975; *Hartmann*, 1984). Impact cratering at many scales, from large basin-forming events to micrometeorite bombardment, also produces characteristic surface roughness features, and the relationship between the two is the subject of the investigations presented here.

The structure of the remaining chapters reflects the two parallel approaches we take to understanding lunar surface roughness and its relation to impact cratering: analysis of high-resolution elevation data from LOLA and forward modeling of cratered terrains. Chapter 2 presents global surface roughness maps using a variety of roughness parameters, including median absolute slope at several scales, median bidirectional slope at the LOLA footprint scale, median differential slope, and Hurst exponent. We explore major regional differences in roughness properties and find that the scale-dependence of lunar surface roughness reveals a change in character at approximately the 1-kilometer scale in the lunar highlands. The next chapter focuses this analysis on several local regions to assess the geologic applications of roughness maps at the lunar south pole, Shackleton crater, and mare surfaces of varying age. Chapter 3 presents a cratered terrain model that we have developed to track both the three-dimensional topography and surviving rim fragments of individual

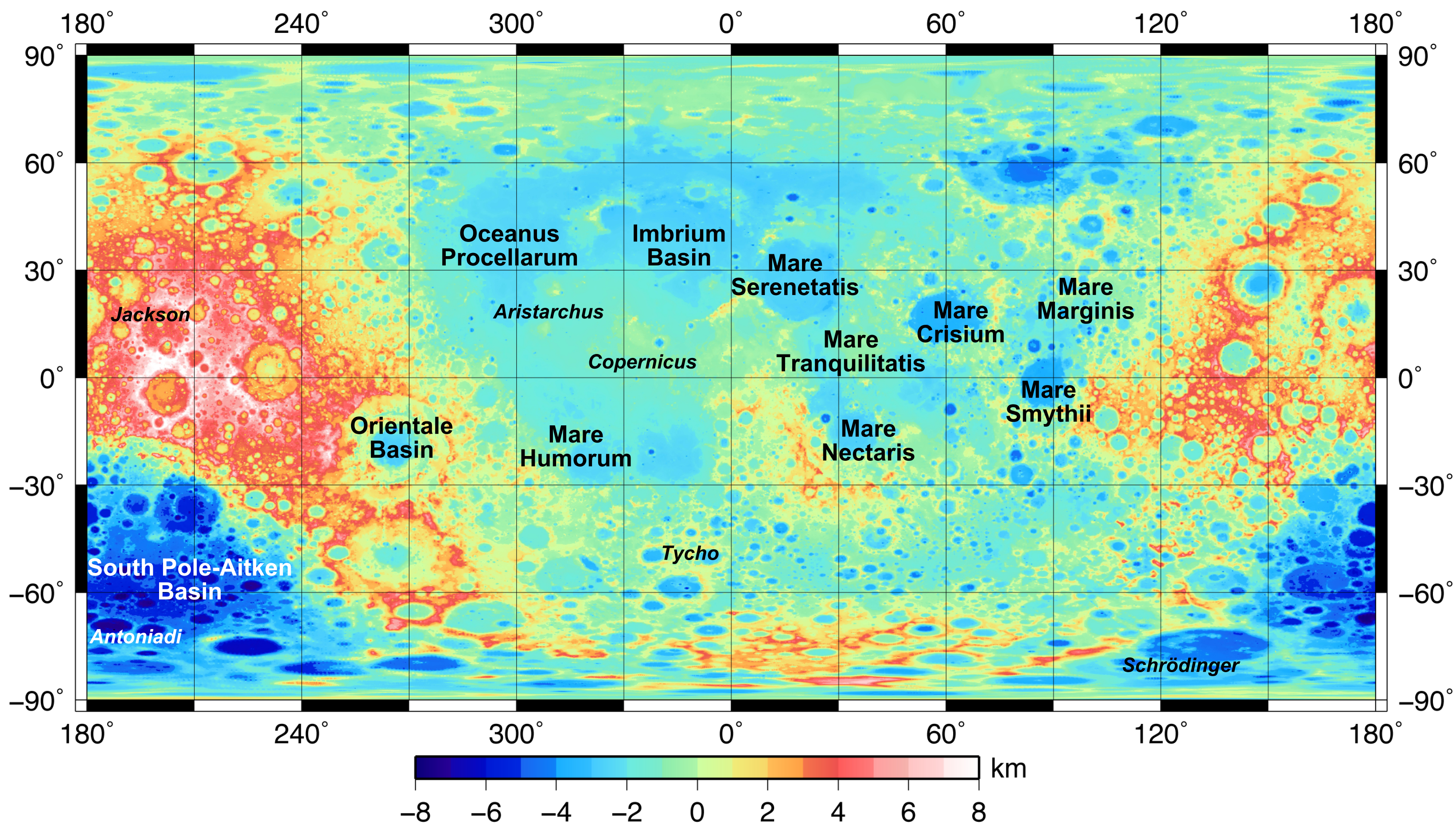

Figure 1.1: Lunar topography from the Lunar Orbiter Laser Altimeter (LOLA) in a simple cylindrical projection, with major basins and relevant features.

craters through time. The dependence of the power spectral density (PSD) on the size-frequency distribution of emplaced craters and the spectral content (shape) of individual craters is explored both analytically and numerically and compared to the PSD along LOLA transects. The final chapter employs the crater rim-tracking capability of the numerical model to investigate the evolution of the size-frequency distribution of "visible" craters as craters accumulate and overlap each other, addressing the geometric bias that results from over- or undercounting large craters and suggesting several potential solutions. Figure 1.1 contains a map of the lunar topography from LOLA that includes major geographical features that are relevant to the work presented in the following chapters.